J. Phys.: Condens. Matter **25** (2013) 316001 (10pp) doi:10.1088/0953-8984/25/31/316001

Ferrimagnetism in $GdCo_{12-x}Fe_xB_6$

L V B Diop[1], O Isnard[1], N R Lee-Hone[2], D H Ryan[2] and J M Cadogan[3]

[1] Institut Néel, CNRS and Université Joseph Fourier, B.P. 166, F-38042 Grenoble Cedex 9, France
[2] Physics Department and Centre for the Physics of Materials, McGill University, Montreal, QC, H3A 2T8, Canada
[3] School of Physical, Environmental and Mathematical Sciences, UNSW Canberra at the Australian Defence Force Academy, Canberra, ACT 2610, Australia

E-mail: olivier.isnard@grenoble.cnrs.fr, S.Cadogan@adfa.edu.au and dhryan@physics.mcgill.ca

Received 3 May 2013, in final form 14 June 2013
Published 9 July 2013
Online at stacks.iop.org/JPhysCM/25/316001

Abstract
The effects of iron substitution on the structural and magnetic properties of the $GdCo_{12-x}Fe_xB_6$ ($0 \leq x \leq 3$) series of compounds have been studied. All of the compounds form in the rhombohedral $SrNi_{12}B_6$-type structure and exhibit ferrimagnetic behaviour below room temperature: T_C decreases from 158 K for $x = 0$ to 93 K for $x = 3$. ^{155}Gd Mössbauer spectroscopy indicates that the easy magnetization axis changes from axial to basal-plane upon substitution of Fe for Co. This observation has been confirmed using neutron powder diffraction. The axial to basal-plane transition is remarkably sensitive to the Fe content and comparison with earlier ^{57}Fe-doping studies suggests that the boundary lies below $x = 0.1$.

(Some figures may appear in colour only in the online journal)

1. Introduction

Transition metal (TM) rich intermetallic compounds are of significant interest as they can combine a large magnetization with a high magnetic ordering temperature. Since the discovery of the high-performance hard magnetic system based on the $Nd_2Fe_{14}B$ phase [1–3], extensive investigations have focused on intermetallic ternary borides combining the magnetic properties of the rare-earth and Co or Fe as the TM element [4–10]. The large amount of interest is driven primarily by the technological importance of these materials. However, there are many fundamental issues, including the nature and composition dependence of exchange interactions, anisotropy and ordering behaviour [11], which need to be investigated in order to better understand the physical properties of the R–Co–B and R–Fe–B systems. The present work is dedicated to an investigation of the fundamental physical properties of the $R(Co, Fe)_{12}B_6$ borides, a family of compounds whose intrinsic magnetic behaviour continues to attract much interest [12–21].

The ternary system $RCo_{12}B_6$ was first identified by Niihara and Yajima [4] and later found to form with iron by Buschow *et al* during a survey of the Nd–Fe–B ternary phase diagram [22]. $RTM_{12}B_6$, where R is a rare-earth element or yttrium and TM is a transition metal (here Co or Fe), crystallizes in the rhombohedral $SrNi_{12}B_6$-type structure ($R\bar{3}m$ #166) [4, 7, 23] in which the TM atoms are located on two inequivalent crystal sites (18g and 18h) with the rare-earth and boron atoms occupying the 3a and 18h sites, respectively. While $NdFe_{12}B_6$ was one of the first iron-based examples of the 1–12–6 family to be discovered [22], it is metastable and $LaFe_{12}B_6$ is the only stable iron-based member of the series [16, 24]. By contrast, the $RCo_{12}B_6$ compounds are stable for essentially all of the rare-earths (with the exception of europium) with lattice parameters that follow the conventional lanthanide contraction [14]. They are all collinear ferro- (R = La–Sm) or ferri- (R = Gd–Tm) magnets with rather small cobalt moments ($\mu_{Co} \sim 0.42\ \mu_B$) and modest ordering temperatures ($T_C \sim 150$ K) [14]. The Co magnetic behaviour has been studied in detail. The itinerant character of the magnetism of this compound has been established [25, 21] and the role of volume has been investigated by magnetization measurements under hydrostatic pressure [26, 19]. NMR studies [25, 27, 28] yielded complex spectra with contributions from cobalt moments in domains and domain walls. The NMR data suggest that the cobalt moments on the two TM sites are different, with the Co(18h) moment being significantly larger

than the Co(18g) moment by a factor of at least 1.3 (based on the ratio of the two hyperfine fields of the domain nuclei) [28]. This difference in the Co moments is driven by the different nearest-neighbour configurations: the 18g site has seven Co neighbours and four B neighbours whereas the 18h site has nine Co and three B neighbours, resulting in a larger moment at the 18h site.

Despite the extensive investigations noted above, there appear to have been no direct measurements of the magnetic structure in this series of compounds. The ferri- or ferro-magnetic ordering has been inferred from bulk magnetization measurements, and the only information on ordering directions comes from ^{57}Fe Mössbauer studies on iron-doped samples of the $RCo_{12}B_6$ compounds. In most cases (Y [18], La [29], Sm [30], Gd [16], Tb [30] and Er [31]) the moments were found to lie in the basal-plane, however two systems (Nd [18] and Ho [32]) exhibit axial ordering at 4.2 K but undergo spin-reorientations to basal-plane ordering on heating through 55 K and 75 K, respectively. Two factors led us to re-evaluate these conclusions. The first is that the ^{57}Fe-doping studies all revealed a very strong preference for iron to occupy the 18h site, where it carries a significantly larger moment (about twice that of the moment of the iron on the 18g site [16]). This is not unusual *per se*, as ^{57}Co-doping of both $Nd_2Fe_{14}B$ [33] and a range of rare-earth/iron binary intermetallic compounds [34] revealed that iron consistently occupies the larger volume sites, with cobalt being more likely to take the smaller sites. The second factor was a marked instability of the iron moment. Magnetization measurements in $LaFe_{12}B_6$ showed a sudden jump at an applied field of about 8.6 T as the iron moment increased by more than a factor of three [24]. This low-moment → high-moment transition can also be driven by adding a magnetic rare-earth such as neodymium [22] or gadolinium [24], where the exchange field acts as a locally applied field and both the iron moment and ordering temperature are greatly increased. Recent tight-binding calculations have confirmed this moment instability and further shown that iron on the 18h site exhibits the greater sensitivity to its environment [35, 20]. Thus, iron systematically substitutes on the site that has the greater sensitivity to its environment. Replacing even a small fraction of the cobalt in $RCo_{12}B_6$ with iron can therefore be expected to have a significant effect on the overall magnetic behaviour of the compound.

We will focus here on the Gd-containing compounds since the 4f shell of gadolinium is spherical ($L = 0$) and consequently one expects no contribution of the Gd atom to the magnetocrystalline anisotropy. As such, the results obtained here should be representative of the TM sublattice only. The composition range studied here, $GdCo_{12-x}Fe_xB_6$, $0 \leq x \leq 3$, was limited by the stability of the $Gd(Co, Fe)_{12}B_6$ system and we could not prepare acceptable samples for $x > 3$. Following a basic structural and magnetic characterization of the materials, we used ^{155}Gd Mössbauer spectroscopy to determine the ordering direction of the Gd moments (and by implication, the direction of the antiparallel TM moments) as a function of the iron doping. We then confirmed the rather surprising doping sensitivity of the ordering by using neutron powder diffraction to study two of the samples ($x = 0$ and 0.5), exploiting a novel large-area flat-plate scattering geometry that mitigates the extreme absorption cross-section of natural gadolinium and permits neutron diffraction on regular samples (no isotopic separation) at thermal wavelengths [36].

2. Experimental methods

2.1. Sample preparation and characterization

The polycrystalline samples were prepared by melting high-purity starting elements (Alfa Aesar, Gd—99.9%, Co—99.95%, Fe—99.99%, B—99.9%) in an induction furnace under a purified argon gas atmosphere. To promote homogeneity, the samples were wrapped in tantalum foil and then annealed at 1173 K for three weeks in evacuated quartz tubes. The crystallographic (phase) purity was checked by x-ray diffraction using a Siemens D5000 diffractometer in reflection mode with the Bragg–Brentano geometry, using Co-Kα radiation, $(K_{\alpha_1}) = 1.789\,00$ Å and $(K_{\alpha_2}) = 1.792\,83$ Å, with a scan step of 0.02° and an angular 2θ range from 20° to 90°. A precise determination of the lattice parameters was obtained by a least-squares refinement of the diffraction patterns, including all the observed Bragg reflections. Following the x-ray diffraction analysis, the sample purity was also checked by carrying out magnetic susceptibility and magnetization measurements. The magnetic measurements were made on powder samples over a wide temperature range from 1.7 to 300 K. The measurements employed the extraction method in an experimental setup that has been described elsewhere [37]. Both isothermal magnetization and the temperature dependence of the susceptibility were measured. The isothermal magnetization curves were recorded in magnetic fields ranging from 0 to 10 T. The ac magnetic susceptibility was measured at a frequency of 10 kHz down to 4 K in a magnetic field of 3 mT.

2.2. Mössbauer spectroscopy

The 50 mCi ^{155}Sm source was prepared by neutron activation of $^{154}SmPd_3$. The source and samples were mounted vertically in a helium flow cryostat and the drive was operated in sinusoidal mode. The 86.55 keV γ-photons used for Mössbauer spectroscopy were isolated from the various x-rays emitted by the source with a high-purity Ge detector. The drive system was calibrated using a laser interferometer with velocities cross checked against both ^{57}Co**Rh**/α-Fe at room temperature and $^{155}SmPd_3/GdFe_2$ at 5 K. Sample temperatures were monitored with a calibrated Cernox thermometer and a stability of better than ±0.01 K was observed. The spectra were fitted using a nonlinear least-squares minimization routine with line positions and intensities derived from an exact solution to the full Hamiltonian [38]. The electric quadrupole coupling constants (ground state) obtained from the fits are referred to as eQV_{zz}.

Table 1. Lattice parameters and unit cell volume for the $GdCo_{12-x}Fe_xB_6$ series of compounds obtained from x-ray diffraction at room temperature.

x (at./f.u.)	0	0.5	1.0	2	3
a (Å)	9.454(1)	9.462(3)	9.468(1)	9.475(1)	9.482(1)
c (Å)	7.449(1)	7.451(1)	7.453(1)	7.457(1)	7.466(1)
V (Å^3)	576.66(10)	577.67(2)	578.58(10)	579.76(06)	581.37(10)

2.3. Neutron diffraction

Neutron diffraction experiments were carried out on the C2 multi-wire powder diffractometer (DUALSPEC) at the NRU reactor, Canadian Neutron Beam Centre, Chalk River, Ontario. To prepare the flat-plate samples for the neutron diffraction measurements ∼700 mg (about a $1/e$ absorption thickness) of finely powdered material was spread across a 2.4 cm by 8 cm area on a 600 μm-thick single-crystal silicon wafer and immobilized using a 1% solution of GE-7031 varnish in toluene/methanol (1:1) [36]. A second silicon wafer was used as a cover. The two plates were mounted in an aluminum frame and loaded into a closed-cycle refrigerator with the sample in a partial pressure of helium to ensure thermal uniformity. The plate was oriented with its surface normal parallel to the incident neutron beam to maximize the total flux onto the sample and the measurements were made in transmission mode. A neutron wavelength (λ) of 1.3286(1) Å was used as no long-period antiferromagnetic ordering modes were expected. All full-pattern magnetic and structural refinements employed the *FullProf/WinPlotr* suite [39, 40] with neutron scattering length coefficients for natural Gd taken from the tabulation by Lynn and Seeger [41]. As all of the key magnetic reflections occurred below $2\theta = 35°$, no absorption correction was applied, however the data were truncated at $2\theta = 50°$ to minimize any possible impact of angle-dependent absorption effects.

3. Results and discussion

3.1. Structural properties

Microprobe analysis performed on the as-cast and annealed samples indicates their high chemical purity. These samples contain a major phase $GdCo_{12-x}Fe_xB_6$ with some amount of the pseudo-binary compound $(Co, Fe)_2B$. In order to minimize the quantity of this additional phase, the nominal compositions of the samples were adjusted, after which the $GdCo_{12-x}Fe_xB_6$ compounds were found to be mainly single phase according to the analysis of the x-ray diffraction patterns. The analysis of the diffraction patterns confirms that the $R\bar{3}m$ (#166) space group symmetry is retained for all the studied compounds. A careful look at the x-ray diffraction patterns indicates the presence of residual traces of the $(Co, Fe)_2B$ impurity. The lattice parameters of the rhombohedral $GdCo_{12}B_6$ compound at room temperature are $a = 9.454(1)$ Å and $c = 7.449(1)$ Å, which are in good agreement with previous results [25, 12, 10, 26, 21, 42, 43]. The lattice parameters for the entire series of samples studied here were obtained from the x-ray diffraction data recorded at room temperature and are summarized in table 1, confirming the presence of a solid solution over the entire composition range studied. Although the cell volume increases linearly as the smaller cobalt is replaced by iron (figure 1), the cell does not expand isotropically and the initial growth in the *ab*-plane is clearly more rapid than that along the *c*-axis (figure 2). As we approach the formation limit of this system, the expansion along the *c*-axis appears to be increasing. This nonlinear anisotropic expansion of the unit cell likely results from the preferential occupation of the 18h site by the substituting iron atoms. Samples with higher iron contents were synthesized, however they were found to contain much larger amounts of the extra phase. This most probably reflects the proximity of the iron solubility limit in the $GdCo_{12-x}Fe_xB_6$ crystal structure. Consequently, those samples with $x > 3$ were not considered further in the present study.

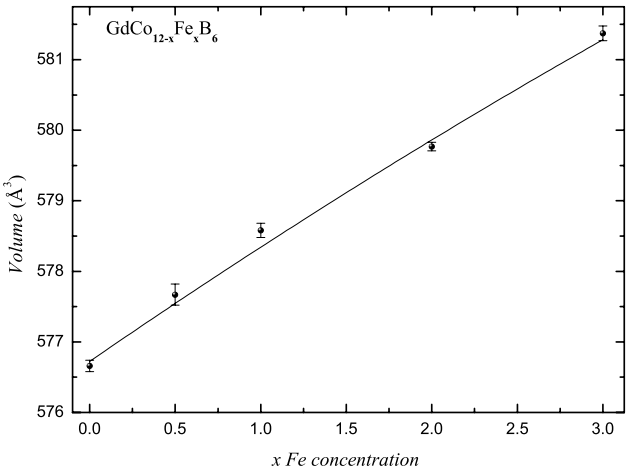

Figure 1. Room temperature cell volume as a function of iron content in $GdCo_{12-x}Fe_xB_6$, showing the expected linear expansion.

3.2. Magnetic properties

The values of the Curie (T_C) and compensation (T_{comp}) temperatures were determined from the temperature dependence of the ac susceptibility (χ') measured in a magnetic field of 3 mT. T_C was taken as the onset of the strong increase seen on cooling, while T_{comp} was defined as the minimum on the $\chi'(T)$ curves observed well below T_C (see figure 3). The parent compound $GdCo_{12}B_6$ exhibits ferrimagnetic behaviour with $T_C = 158$ K and $T_{comp} = 50$ K. As can be seen from figure 4, T_C decreases monotonically from 158 K for $x = 0$ to 93 K for $x = 3$, while T_{comp} passes

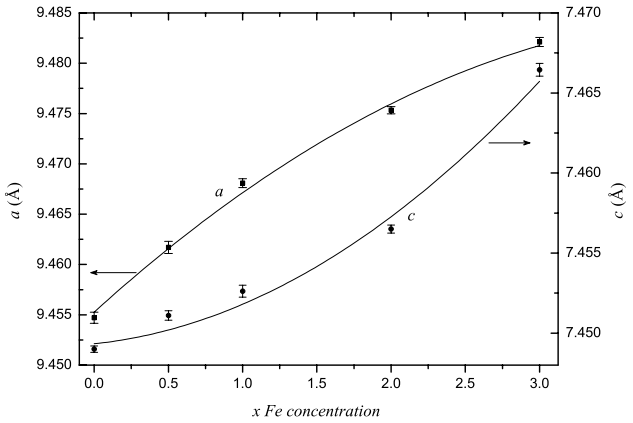

Figure 2. Lattice parameters of $GdCo_{12-x}Fe_xB_6$ obtained from refinement of room temperature x-ray diffraction data, showing the anisotropic expansion of the unit cell as iron preferentially substitutes for cobalt on the 18h site.

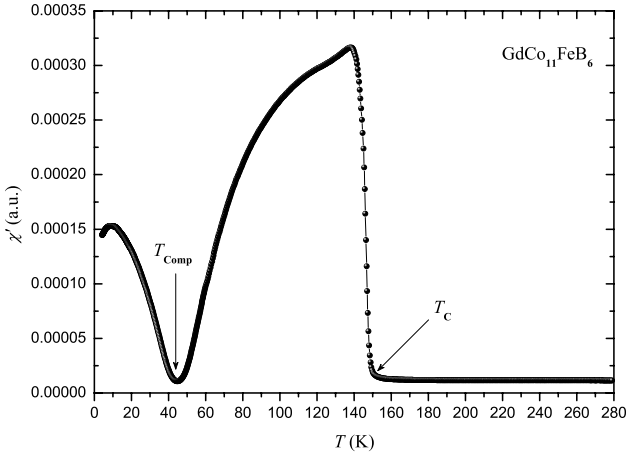

Figure 3. AC susceptibility (χ') measured at a frequency of 10 kHz in a magnetic field of 3 mT for $GdCo_{11}FeB_6$, showing the onset of order at $T_C = 148$ K and the compensation point at $T_{comp} \sim 44$ K.

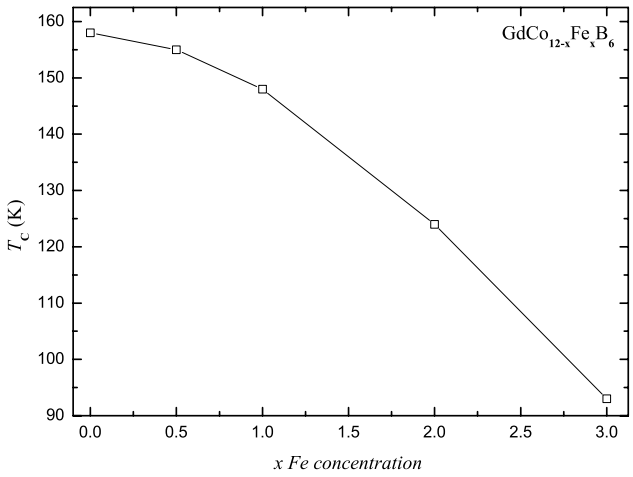

Figure 4. T_C versus x for $GdCo_{12-x}Fe_xB_6$, showing the steady decline with increasing iron doping.

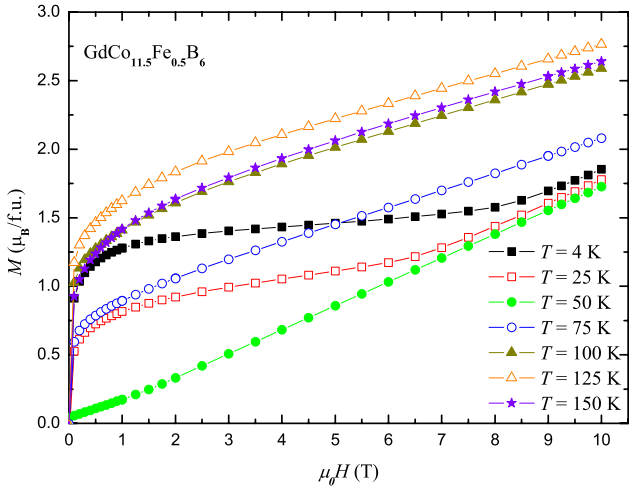

Figure 5. Magnetization curves for $GdCo_{11.5}Fe_{0.5}B_6$ between 4 and 150 K.

through a shallow minimum near $x = 1$ and then increases (table 2). Figure 5 shows the low-temperature magnetization curves for $GdCo_{11.5}Fe_{0.5}B_6$. It is clear that the spontaneous magnetization decreases from 4 to 50 K then increases with increasing temperature, reaching a maximum around 125 K before decreasing again when approaching the Curie temperature. This behaviour is typical of a ferrimagnetic compound exhibiting a compensation temperature near 50 K. This interpretation is confirmed by the analysis of the temperature dependence of the susceptibility as shown in figure 3. Indeed the curve recorded for the $x = 1$ compound clearly exhibits a compensation of the magnetization of the Gd and (Fe, Co) sublattices close to 44 K. Another remarkable feature of the magnetization curve is the large susceptibility at high magnetic field; this large slope is characteristic of the antiparallel coupling of the Gd and (Fe/Co) sublattices which leads to a progressive tilting of these sublattices under the external applied magnetic field. Such properties have been extensively investigated using much higher magnetic fields [21]. However, the complete saturation of the magnetization into a field-induced ferromagnetic state occurs at very high field, i.e. close to 70 T for $GdCo_{12}B_6$. Such values were inaccessible with the experimental setup used here.

The macroscopic intersublattice coupling constant ($n_{Gd\text{-}3d}$) can be obtained from the linear part of the high-field magnetization curves of ferrimagnetic compounds as described previously [44, 45]. Using the magnetization curves plotted in figure 5 we derived a value of $n_{Gd\text{-}3d} = 5.87 \pm 0.13$ T f.u. μ_B^{-1} at 4 K for $x = 0.5$ compared to $n_{Gd\text{-}3d} = 5.19 \pm 0.15$ T f.u. μ_B^{-1} for the undoped $GdCo_{12}B_6$ compound. Converting these values into exchange integrals $J_{(Gd-3d)/k_B}$ one gets -5.26 ± 0.12 K and -4.65 ± 0.14 K for $x = 0.5$ and $x = 0$ respectively. It is worth mentioning that $n_{Gd\text{-}3d}$ continues to increase as more iron is added, being 6.0 ± 0.17 K for $x = 1$ and 6.40 ± 0.20 K for $x = 3$. A more precise determination of this parameter can be performed using high magnetic field measurements and are reported elsewhere [46].

Table 2. Magnetic parameters: Curie temperature, compensation temperature and spontaneous magnetization for the $GdCo_{12-x}Fe_xB_6$ series of compounds obtained from ac susceptibility measurements and isothermal magnetization curves.

$GdCo_{12-x}Fe_xB_6$	T_C (K)	T_{comp} (K)	M_S (μ_B/f.u.)	μ_{TM} (μ_B/TM)	μ_{Fe} (μ_B/Fe)
$x = 0$	158	47.5	1.68(4)	0.443(3)	—
$x = 0.5$	155	45	1.30(5)	0.475(4)	1.3(1)
$x = 1$	148	44.5	1.13(5)	0.489(4)	1.03(5)
$x = 2$	124	46.5	0.99(6)	0.501(5)	0.81(3)
$x = 3$	93	52	0.89(6)	0.510(5)	0.72(2)

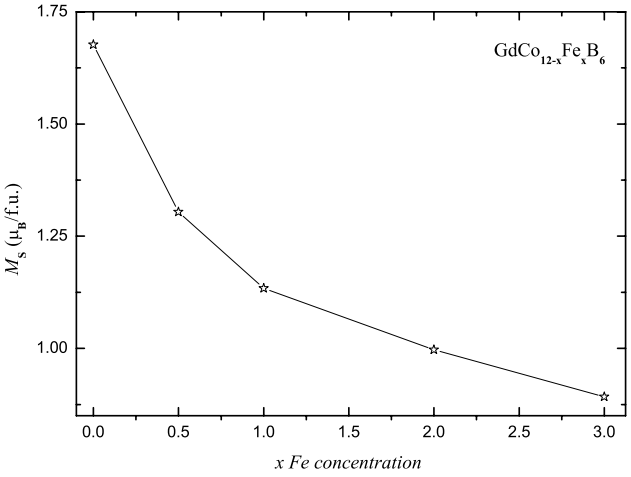

Figure 6. The spontaneous magnetization (M_S) of $GdCo_{12-x}Fe_xB_6$ at 4 K.

The spontaneous magnetization (M_S) for each sample was obtained by a linear extrapolation of the isothermal magnetization curves to $\mu_0 H = 0$ T. Values were corrected for the presence of the $(Co, Fe)_2B$ impurity phase noted earlier. Two methods were used to determine the amount of impurity present: (i) x-ray diffraction analysis and (ii) magnetization measurements. The latter measurements were performed just above the Curie temperature of the compounds studied here (ranging from 100 to 170 K) in order to remain far below the ordering temperature of $(Fe, Co)_2B$, which ranges from 1015 to 429 K. The estimated impurity concentration increases from about 2 wt% up to 6 wt% for $x = 0$ and $x = 3$, respectively. M_S at 4 K shows a monotonic decrease with increasing Fe concentration from 1.68 μ_B/f.u. to 0.89 μ_B/f.u. as x increases from 0 to 3, as shown in figure 6. The corresponding values are summarized in table 2. Assuming that the Gd atom carries its free-ion moment of 7 μ_B, the average transition metal magnetic moment μ_{TM} can be obtained by using $M_S = |(12\ \mu_{TM} - \mu_{Gd})|$. The derived value of $\mu_{TM} = 0.44\ \mu_B$ for the $x = 0$ sample is typical of that found in the $RCo_{12}B_6$ system [14]. If we then write μ_{TM} as $\mu_{TM} = ((12 - x)/12)\mu_{Co} + (x/12)\mu_{Fe}$ and further assume that the cobalt moment (μ_{Co}) can be considered fixed, then we can obtain the estimates for the iron moments (μ_{Fe}) in these compounds shown in table 2. The fact that the calculated Fe moment decreases with increasing Fe content, as shown in table 2, suggests that the *a priori* assumption of a constant Co moment is probably invalid. Nevertheless, it is clear that both μ_{Co} and μ_{Fe} are very low in these compounds, an observation that is most likely due to electronic hybridization with the boron atoms. It is also clear that the iron moments are significantly larger than those of cobalt, which is consistent with the 1.37 μ_B/Fe reported for metastable $NdFe_{12}B_6$ [22, 16], $GdCo_{11.8}Fe_{0.2}B_6$, where an iron moment $\gtrsim 1\ \mu_B$ can be estimated [16], and Gd-doped $La_{1-x}Gd_xFe_{12}B_6$ (1.6 μ_B/Fe for $x > 0.3$) [24].

3.3. ^{155}*Gd Mössbauer results*

While it is clear from the magnetization and susceptibility data presented above that the Gd and TM moments order antiparallel to each other, forming a simple ferrimagnetic structure, bulk measurements cannot provide any direct information regarding the orientation of the moments within the unit cell. As noted above, all current information on the ordering directions in the $RCo_{12}B_6$ compounds comes from ^{57}Fe Mössbauer studies on iron-doped samples and no direct measurements appear to have been made by neutron diffraction, perhaps as a result of the rather simple magnetic structures expected, or the perceived difficulties associated with the neutron absorption by the large amount of boron present. We therefore turned to ^{155}Gd Mössbauer spectroscopy, which can be used to determine the orientation of the gadolinium moments with respect to the principal axis system of the electric field gradient (efg) tensor.

As discussed in our recent paper [47], the hyperfine magnetic field (B_{hf}) at the Gd site is almost entirely due to the local contribution of the Gd moment. Therefore, B_{hf} is collinear with the Gd moment and the fitted angle (θ) between the principal axis of the efg and B_{hf} is a direct measurement of the angle between the Gd moments and the crystallographic c-axis. (The $\bar{3}m$ point symmetry of the Gd(3a) site guarantees an axially symmetric efg tensor ($\eta = 0$) with its principal axis aligned along the crystallographic c-axis [48].)

The full set of ^{155}Gd Mössbauer spectra of $GdCo_{12}Fe_xB_6$ ($0 \leq x \leq 3$), acquired at 5 K in the magnetically ordered state in the saturated regime, were presented in our previous paper [47]. Both the hyperfine field (B_{hf}) and the quadrupole coupling constant (eQV_{zz}) were found to be smooth functions of the Fe content [47]. The hyperfine field decreases linearly from 26.0(2) T for $GdCo_{12}B_6$ to 23.9(2) T for $GdCo_9Fe_3B_6$, while $-eQV_{zz}$ increases from 1.31(3) to 1.84(4) mm s^{-1}. These changes are consistent with the simple evolution of the magnetic properties noted in the bulk characterization above.

However, it is immediately apparent from a visual inspection of the spectra in figure 7 that there is a large difference between the spectra of the undoped $GdCo_{12}B_6$ and the doped sample. This is clearly seen in the asymmetry of the

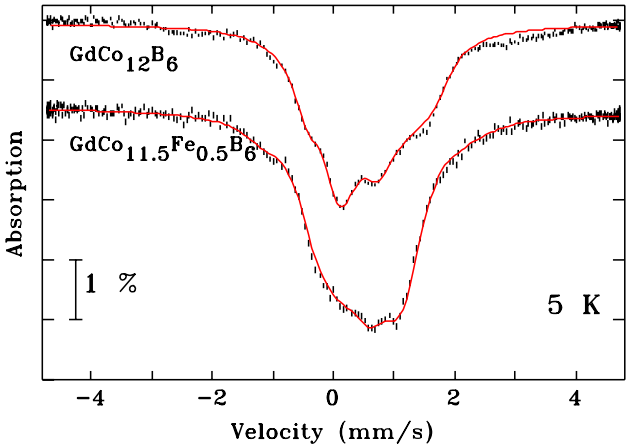

Figure 7. ^{155}Gd Mössbauer spectra of $GdCo_{12-x}Fe_xB_6$ and $GdCo_{11.5}Fe_{0.5}B_6$, showing the clear change in spectral shape upon Fe-doping. Solid lines are the fits to the full Hamiltonian described in the text.

spectra. Our x-ray diffraction work rules out a major structural distortion as the origin of the changes in figure 7 and the fitted Mössbauer parameters [47] reveal that the change in spectral shape is due to a dramatic change in the orientation of the Gd moments, rather than changes in either the hyperfine field or the quadrupole coupling constant (eQV_{zz}). The fitted value of θ shows that, in $GdCo_{12}B_6$, the Gd moments order close to the c-axis ($\theta \sim 15° \pm 2°$), while they are almost perpendicular to the c-axis for $GdCo_{12-x}Fe_xB_6$ with $x \geq 0.5$.

While the origin of the misfit in the spectrum of $GdCo_{12}B_6$ apparent in figure 7 is unclear, it does not affect our conclusion about the canting angle θ. As we will show below, the result is fully supported by neutron diffraction. Attempts to include a contribution from either $GdCo_2B_2$ [49] or $GdCo_3B_2$ [50] were unsuccessful, as while they did reduce χ^2 for the fit, they occupied ∼10% of the spectral area (an unrealistic level of impurity that can be ruled out immediately from x-ray data), and acted to *lower* the canting angle to close to 10°. Our best fit using a fictitious impurity ($B_{hf} = 8(2)$ T, $eQV_{zz} = -11.3(1)$ mm s^{-1}) requires 6% of the spectral area (far too much to be consistent with our x-ray diffraction data) and does not change the value of the canting angle from 15°.

The lowest doping level used here ($x = 0.5$) corresponds to replacing ∼4% of the cobalt by iron, making the ordering direction remarkably sensitive to iron doping. However, the actual sensitivity may be far greater. Indeed, Rosenberg *et al* [16] replaced only 2% of the cobalt with iron in their earlier ^{57}Fe-doping work and interpreted their ^{57}Fe Mössbauer spectrum as showing basal-plane ordering. A later study of a sample doped with only 0.5% ^{57}Fe (∼0.06 Fe/f.u.) also suggested planar ordering [51]. Thus, *only* $GdCo_{12}B_6$ exhibits axial ordering and the $GdCo_{12-x}Fe_xB_6$ system is remarkably sensitive to iron doping with the axial–basal boundary lying somewhere below 0.5% Fe-doping (∼0.06 Fe/f.u.).

While the fits to the ^{155}Gd Mössbauer spectra yield ordering angles that differ from those expected for simple axial and planar ordering by many standard deviations and are therefore statistically significant, it is not immediately clear whether these departures should be considered real, especially in the case of $GdCo_{12}B_6$, where there is no disorder or obvious departures from symmetry that might lead to a canted structure. We turn therefore to neutron diffraction for a final and direct determination of the magnetic ordering direction within the crystal cell.

3.4. Neutron diffraction results

To the best of our knowledge, no member of the $RCo_{12}B_6$ family has been studied using neutron diffraction, possibly as a result of the perceived difficulties associated with working with materials that contain so much highly absorbing boron ($\sigma_{abs} = 767$ b). While this problem could be avoided by using ^{11}B in making the samples, the simple magnetic structures expected might not have justified the additional effort. Gadolinium is substantially more absorbing than boron (the six boron atoms contribute about 10% of the total absorption in $GdCo_{12}B_6$, the rest being due to the single gadolinium atom) and this system would not normally be the starting point for an investigation of magnetic ordering in $RCo_{12-x}Fe_xB_6$; indeed, almost any other rare-earth would be preferable. However, since we have found indications of a remarkable sensitivity to doping in the gadolinium series, we used the same samples for neutron diffraction.

While the large thermal (∼50 000 b) neutron absorption cross-section of natural gadolinium certainly makes neutron diffraction measurements somewhat challenging, they are by no means impossible and frequently yield essential information. We developed a simple large-area flat-plate technique [36] and have now used it to study a wide variety of gadolinium [52–54], europium [55, 56] and samarium [57] compounds. As can be seen in figure 8, $GdCo_{12}B_6$ yields clear neutron diffraction patterns. The contribution of the magnetic order to the diffraction patterns is most clearly reflected in the relative intensities of the (101) peak, at $2\theta = 13.9°$, and the (110) peak at $2\theta = 16.2°$. Fitting the 3.6 K pattern yields the results presented in table 3. Two important features stand out. The first is that the moments are indeed canted away from the c-axis, by 38(8)°, confirming the results of the ^{155}Gd Mössbauer analysis but giving a larger canting angle. The second is that the cobalt moment in the 18h site is slightly larger than that in the 18g site, consistent with NMR work [25, 28].

The diffraction pattern of the $GdCo_{11.5}Fe_{0.5}B_6$ sample at 3.6 K shown in figure 9 immediately confirms that the moments are not oriented the same way as they are in $GdCo_{12}B_6$. The intensity of the (101) peak is more than twice that of the (110) peak, indicating a more planar character to the ordering. This is confirmed by a fit to the diffraction pattern that yields a canting angle of 90°, i.e. in the *ab*-plane, fully consistent with the ^{155}Gd Mössbauer analysis of this sample (figure 10).

We note that the two canting angles for $GdCo_{12}B_6$ derived from Mössbauer spectroscopy (15(2)°) and neutron diffraction (38(8)°) do not agree within error. Examination of χ^2 versus canting angle for the neutron diffraction fits reveals

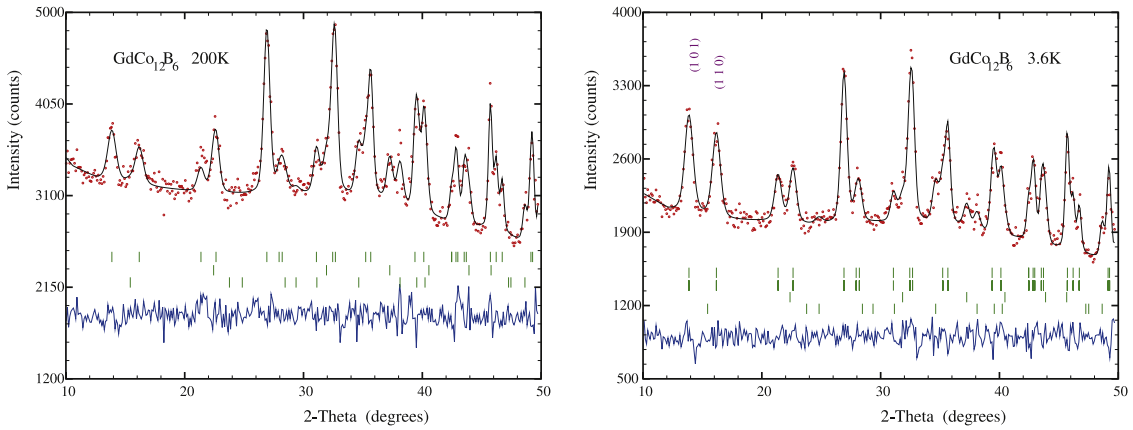

Figure 8. Refinements of the neutron diffraction patterns for $GdCo_{12}B_6$ taken at 200 K (top) and 3.6 K (bottom), above and below T_C respectively. The (101) and (110) peaks are identified on the 3.6 K pattern. The top row of Bragg markers is for the $GdCo_{12}B_6$ primary phase, with a second row shown for the Co_2B impurity.

Table 3. Lattice parameters, atomic coordinates, magnetic moments and moment orientations extracted from the refinements of the powder neutron diffraction patterns. The angle of the moments in $GdCo_{11.5}Fe_{0.5}B_6$ refines to 90°, but *Fullprof* provides no meaningful error estimate. Parameters without error values were kept fixed during the refinements.

	$GdCo_{12}B_6$		$GdCo_{11.5}Fe_{0.5}B_6$	
Temperature (K)	200	4	200	4
a (Å)	9.444(7)	9.435(7)	9.446(7)	9.440(7)
c (Å)	7.437(5)	7.442(5)	7.436(5)	7.443(5)
Co (18g)				
x	0.409(5)	0.409	0.415(5)	0.415
Co (18h)				
x	0.433(4)	0.433	0.428(4)	0.428
z	0.058(6)	0.058	0.060(2)	0.060
B (18h)				
x	0.480(2)	0.480	0.483(3)	0.483
z	0.296(5)	0.296	0.292(6)	0.292
Gd moment (μ_B)	0	6.9(5)	0	6.9
18g TM moment (μ_B)	0	0.41(3)	0	0.22(5)
18h TM moment (μ_B)	0	0.50(3)	0	0.71(7)
Moment—*c*-axis angle (deg)	—	38(8)	—	90
R(Bragg)	7.5	3.9	9.8	6.9
R(F)	3.9	2.2	5.4	4.0
R(Mag)	—	5.4	—	6.3
χ^2	2.82	2.36	3.20	3.06

that, while 30°–40° is indeed the minimum, the function is very weakly curved at low angles and forcing $\theta = 15°$ only increases χ^2 by 2%. Given the greater sensitivity of the Mössbauer data in this region, we take the angle derived from the neutron diffraction as support for approximately axial ordering, rather than an absolute determination of the canting angle.

Even within the limitations noted here and in the discussion of the Mössbauer results, the basic conclusion is clear: The moments in $GdCo_{12}B_6$ order close to the *c*-axis, but are definitely canted away from this axis by at least 15°, while in $GdCo_{11.5}Fe_{0.5}B_6$ the moments lie in the *ab*-plane.

3.5. Discussion

The refinement of the magnetic pattern of the Fe-doped sample at 3.6 K is extraordinarily sensitive to the transition metal (TM) magnetic moments and the canting angle. We arrived at the canting angle of 90° by monitoring the behaviour of the χ^2 goodness-of-fit parameter with all moments fixed. Acceptable fits were obtained with a Co(18g) moment of 0.41(5) μ_B, as found in the undoped sample, and an 18h moment of 0.61(4) μ_B, yielding an average TM moment of 0.51(6) μ_B, consistent with the magnetometry results in table 2. However, the refinement process showed a clear tendency to reduce the 18g moment in the Fe-doped sample significantly while increasing the 18h moment. By reducing the 18g moment to 0.22(5) μ_B (from 0.41 μ_B) and increasing the 18h moment to 0.71(7) μ_B, the χ^2 decreased from 3.24 to 3.06. Once again, an average TM moment of 0.47(9) μ_B was obtained, in excellent agreement with the magnetometry results in table 2.

Given the data quality, it is difficult to say whether or not this reduction is real. It is possible that the two Co sites

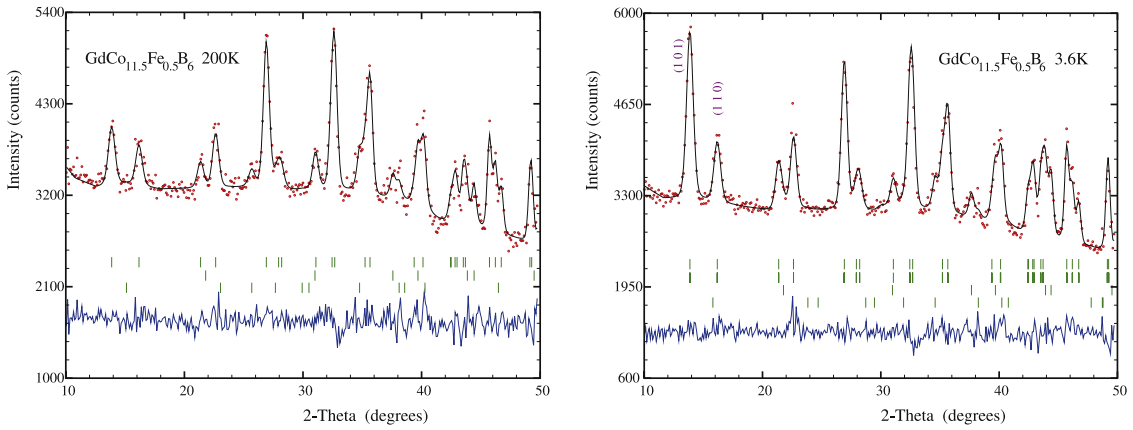

Figure 9. Refinements of the neutron diffraction patterns for $GdCo_{11.5}Fe_{0.5}B_6$ taken at 200 K (top) and 3.6 K (bottom), above and below T_C respectively. The (101) and (110) peaks are identified on the 3.6 K pattern. The top row of Bragg markers is for the $GdCo_{12}B_6$ primary phase, with a second row shown for the Co_2B impurity.

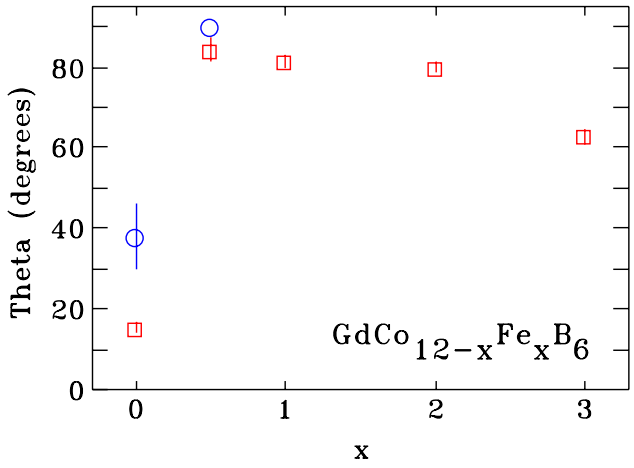

Figure 10. Composition dependence of the canting angle in $GdCo_{12-x}Fe_xB_6$ derived from ^{155}Gd Mössbauer spectroscopy (□) and neutron diffraction (○).

in the 1:12:6 structure have opposing anisotropies and this behaviour of the TM moments may reflect opposing orbital effects associated with the change in ordering direction.

It is well established that the two Co sites in the YCo_4B structure, for example, do have opposing anisotropies and the effects of this competition, leading to a spin-reorientation, have been observed by ^{57}Fe Mössbauer spectroscopy [58] on YCo_4B doped with enriched ^{57}Fe and also by ^{59}Co NMR [59].

Furthermore, there is considerable experimental evidence to suggest that the anisotropy behaviours of the Co and Fe sublattices in TM-rich intermetallics have opposite signs. For example, in the $R_2TM_{14}B$ series, $Y_2Fe_{14}B$ shows easy-axis order whereas $Y_2Co_{14}B$ is easy-plane. Similar behaviour is observed in the $R(TM, X)_{12}$ compounds with X = V and Si. The opposite competitive behaviour, i.e. axial order for Co and planar order for Fe, is observed in $Y_2TM_{17}N_x$ [60].

Work on R-(Co, Fe)-based intermetallics shows that very little Fe substitution is needed to alter the magnetic anisotropy of Co-rich compounds when there are two or more Co sites with competing anisotropies. This is particularly the case when the Fe shows a distinct site occupancy preference, as we observe here in the $R(Co, Fe)_{12}B_6$ system. For example, in the $Y(Co, Fe)_4B$ series a 0.75% replacement of Co by Fe is sufficient to increase the spin-reorientation temperature T_{SR} from 145 to 165 K. Further replacement leads to a T_{SR} of 225 K for 2% Fe on the TM sublattice [61].

A spin-reorientation of opposite character has been reported as high as 450 K for the Fe-rich side, where $YCoFe_3B$ exhibits a change from axial ordering below T_{SR} to basal-plane ordering above T_{SR} [62].

Electronic structure calculations [63, 64] on $Y(Co, Fe)_5$ reproduce the different signs of the anisotropies exhibited by Co and Fe. If we consider the parent compound YCo_5 it is clear that the two Co sites (2c and 3g) have opposing anisotropies. Polarized neutron diffraction work [65] and NMR [66] show that the magnetic behaviour of YCo_5 is dictated by the Co(2c) site, which has a large orbital contribution to its magnetic moment and hence a large anisotropy.

Therefore, we suggest that the dramatic effect that Fe substitution has on the magnetic ordering in $Gd(Co, Fe)_{12}B_6$ is related to the strong preference Fe has to occupy the 18h TM site and may reflect competing anisotropies of the 18g and 18h Co sites, which would fit in well with the fact that only very small amounts of Fe are sufficient to drive the magnetic ordering from easy-axis to easy-plane. We are currently pursuing these ideas with other $R(Co, Fe)_{12}B_6$ samples which do not contain the extreme neutron absorber gadolinium.

4. Conclusions

The rhombohedral crystal structure of the $GdCo_{12-x}Fe_xB_6$ compounds is preserved at least as far as $x = 3$. The substitution of Fe for Co leads to a pronounced lattice expansion and a progressive decrease in the Curie temperature. The compensation temperature is only weakly affected and the moments on the Gd and Co, Fe sublattices cancel at about 50 K for all x. ^{155}Gd Mössbauer spectroscopy demonstrates that a very low iron content is sufficient to induce a reorientation of the easy magnetization

direction in the $GdCo_{12-x}Fe_xB_6$ compounds. This large effect occurs in spite of relatively moderate effects on magnetic properties such as spontaneous magnetization and compensation temperature. This reorientation was confirmed using neutron powder diffraction. Comparison with earlier ^{57}Fe Mössbauer work on ^{57}Fe-doped samples suggests that the axial to basal-plane boundary lies below $x = 0.1$. Given that essentially all of the ordering directions reported in the $RCo_{12}B_6$ system have been derived from Fe-doped samples, these assignments need to be re-evaluated in light of the demonstrated sensitivity of the ordering direction to doping with iron.

Acknowledgments

We gratefully acknowledge the assistance of Raghu Rao and Robert Speranzini in arranging for the activation of the ^{155}Gd Mössbauer source in the National Research Universal (NRU) research reactor, which is operated by Atomic Energy of Canada, Ltd, at Chalk River, Ontario. DHR and NRL-H were supported by grants from the Natural Sciences and Engineering Research Council of Canada and Fonds Québécois de la Recherche sur la Nature et les Technologies. JMC acknowledges support from the University of New South Wales.

References

[1] Sagawa M, Fujimura S, Togawa N, Yamamoto H and Matsuura Y 1984 *J. Appl. Phys.* **55** 2083
[2] Herbst J F, Croat J J, Pinkerton F E and Yelon W B 1984 *Phys. Rev.* B **29** 4176–8
[3] Givord D, Li H S and Moreau J M 1984 *Solid State Commun.* **50** 497–9
[4] Niihara K and Yajima S 1972 *Chem. Lett.* **1** 875–6
[5] Chaban N F and Kuz'ma Yu B 1977 *Isv. Akad. Nauk. SSSR Neorg. Mater.* **13** 923–4
[6] Stadelmaier H H and Lee H J 1978 *Z. Metallk.* **69** 685–9
[7] Kuz'ma Yu B, Chernyak G V and Chaban N F 1981 *Dopov. Akad. Nauk. Ukr. RSR* **12** 81–4
[8] Kuz'ma Yu B, Bilonizhko N S, Chaban N F and Chernyak G V 1983 *J. Less-Common Met.* **90** 217–22
[9] Chen Y, Liang J, Chen X and Liu Q 2000 *J. Alloys Compounds* **296** L1–3
[10] Cordier G, Klemens R and Albert B 2007 *Z. Anorg. Allg. Chem.* **633** 1603–7
[11] Franse J J M and Radwański R J 1993 Magnetic properties of binary rare-earth 3d-transition-metal intermetallic compounds *Handbook of Magnetic Materials* vol 7, ed K H J Buschow (Amsterdam: Elsevier) pp 307–501 chapter 5
[12] Jurczyk M, Pedziwiatr A T and Wallace W E 1987 *J. Magn. Magn. Mater.* **67** L1–3
[13] Rosenberg M, Mittag M and Buschow K H J 1988 *J. Appl. Phys.* **63** 3586–8
[14] Mittag M, Rosenberg M and Buschow K H J 1989 *J. Magn. Magn. Mater.* **82** 109–17
[15] Zhou G F, Li X, de Boer F R and Buschow K H J 1992 Field-induced transitions in $RCo_{12}B_6$ compounds *Physica* B **177** 286–90
[16] Rosenberg M, Sinnemann T, Mittag M and Buschow K H J 1992 *J. Alloys Compounds* **182** 145–56
[17] Zhou G F, Li X, de Boer F R and Buschow K H J 1992 *J. Magn. Magn. Mater.* **109** 265–70
[18] Cadogan J M, Campbell S J, Zhao X L and Wu E 1993 *Aust. J. Phys.* **46** 679
[19] Arnold Z, Isnard O, Mayot H, Míšek M and Kamarád J 2010 *J. Magn. Magn. Mater.* **322** 1117–9
[20] Miletić G I and Blažina Ž 2011 *J. Magn. Magn. Mater.* **323** 2340–7
[21] Isnard O, Skourski Y, Diop L V B, Arnold Z, Andreev A V, Wosnitza J, Iwasa A, Kondo A, Matsuo A and Kindo K 2012 *J. Appl. Phys.* **111** 093916
[22] Buschow K H J, de Mooij D B and van Noort H M 1986 *J. Less-Common Met.* **125** 135–46
[23] Jung W and Quentmeier D 1980 *Z. Kristallogr.* **151** 121–8
[24] Li Q A, de Groot C H, de Boer F R and Buschow K H J 1997 *J. Alloys Compounds* **256** 82–5
[25] Erdmann K, Rosenberg M and Buschow K H J 1988 *J. Appl. Phys.* **63** 4113–5
[26] Arnold Z, Isnard O, Mayot H, Skorokhod Y, Kamarád J and Míšek M 2012 *Solid State Commun.* **152** 1164–7
[27] Nagahama M, Satohira S I, Akazawa T, Nakamura F, Fujita T and Kawakami M 1991 *J. Phys. Soc. Japan* **60** 3855
[28] Kawakami M and Satohira S 1992 *J. Magn. Magn. Mater.* **104–107** 1313–4 Part 2 (0)
[29] Wu E, Cadogan J M, Campbell S J and Zhao X L 1994 *Hyperfine Interact.* **94** 1903–8
[30] Zhao X L, Campbell S J, Cadogan J M, Li H-S and Thompson P W 1996 *ICAME 1995, SIF Conf. Proc.* vol 50 pp 211–4
[31] Zhao X, Cadogan J M and Campbell S J 1995 *J. Magn. Magn. Mater.* **140–144** 959–60 Part 2 (0)
[32] Cadogan J M, Campbell S J, Zhao X L, Li H S and Thompson P W 2002 Spin reorientation in $HoCo_{12}B_6$ *Hyperfine Interactions (C)* (*Proc.* vol 5) ed M F Thomas, J M Williams and T C Gibb, pp 119–22
[33] Ryan D H, Altounian Z, Ström-Olsen J O and Muir W B 1989 *Phys. Rev.* B **39** 4730
[34] Liao L X, Altounian Z and Ryan D H 1993 *Phys. Rev.* B **47** 11230
[35] Miletić G I and Blažina Ž 2007 *J. Alloys Compounds* **430** 9–12
[36] Ryan D H and Cranswick L M D 2008 *J. Appl. Crystallogr.* **41** 198–205
[37] Barlet A, Genna J C and Lethuillier P 1991 *Cryogenics* **31** 801–5
[38] Voyer C J and Ryan D H 2006 *Hyperfine Interact.* **170** 91–104
[39] Rodríguez-Carvajal J 1993 *Physica* B **192** 55
[40] Roisnel T and Rodríguez-Carvajal J 2001 *Mater. Res. Forum* **378–381** 118
[41] Lynn J E and Seeger P A 1990 *At. Data Nucl. Data Tables* **44** 191–207
[42] Lee S P, Kim C K, Nahm K, Mittag M, Jeong Y H and Ryu C-M 1997 *J. Appl. Phys.* **81** 2454–6
[43] Nahm K, Kim C K, Mittag M and Jeong Y H 1995 *J. Appl. Phys.* **78** 3980–2
[44] Yang F, Wang J, Gao Y, Tang N, Han X, Pan H, Qingan L, Hu J, Liu J P and de Boer F R 1996 *J. Appl. Phys.* **79** 7883
[45] Wang J L, Campbell S J, Tegus O, Marquina C and Ibarra M R 2007 *Phys. Rev.* B **75** 174423
[46] Diop L V B, Isnard O, Skourski Y and Ballon G 2013 *J. Appl. Phys.* **113** 203911
[47] Lee-Hone N R, Ryan D H, Isnard O, Diop L V B and Cadogan J M 2013 *J. Appl. Phys.* **113** 17E119
[48] Stewart G A 1994 Some applications of rare earth Mössbauer spectroscopy *Materials Forum* **18** 177–93
[49] Felner I 1984 *Solid State Commun.* **52** 191–5
[50] Buschow K H J, Coehoorn R, Mulder F M and Thiel R C 1993 *J. Magn. Magn. Mater.* **118** 347–51
[51] Zhao X 1996 *PhD Thesis* UNSW, Australia

[52] Cadogan J M, Ryan D H, Napoletano M, Riani P and Cranswick L M D 2009 *J. Phys.: Condens. Matter* **21** 124201
[53] Ryan D H, Cadogan J M, Cranswick L M D, Gschneidner K A Jr, Pecharsky V K and Mudryk Y 2010 *Phys. Rev.* B **82** 224405
[54] Ryan D H, Lee-Hone N R, Cadogan J M, Canfield P C and Bud'ko S L 2011 *J. Phys.: Condens. Matter* **23** 106003
[55] Ryan D H, Cadogan J M, Xu S, Xu Z and Cao G 2011 *Phys. Rev.* B **83** 132403
[56] Lemoine P, Cadogan J M, Ryan D H and Giovannini M 2012 *J. Phys.: Condens. Matter* **24** 236004
[57] Ryan D H, Cadogan J M, Ritter C, Canepa F, Palenzona A and Putti M 2009 *Phys. Rev.* B **80** 220503
[58] Cadogan J M, Li H S, Campbell S J and Jing J 1992 *Solid State Commun.* **81** 121–3
[59] Kapusta Cz, Spridis N and Figiel H 1990 *J. Magn. Magn. Mater.* **83** 153–4
[60] Buschow K H J, Hu S J, Tegus O, Zhang L, Brück E and de Boer F R 2001 *J. Alloys Compounds* **317/318** 2–7
[61] Dung T T, Thuy N P, Hong N M, Hien T D and Franse J J M 1991 *J. Appl. Phys.* **69** 4633–5
[62] Grandjean F, Sougrati M T, Mayot H, Isnard O and Long G J 2009 *J. Phys.: Condens. Matter* **21** 186001
[63] Trygg J, Nordström L and Johansson B 1993 *Int. J. Mod. Phys.* **7** 745–8
[64] Yamada H, Terao K, Nakazawa H, Kitagawa I, Suzuki N and Ido H 1998 *J. Magn. Magn. Mater.* **183** 94–100
[65] Déportes J, Givord D, Schweizer J and Tasset F 1976 *IEEE Trans. Magn.* **12** 1000–2
[66] Streever R L 1979 *Phys. Rev.* B **19** 2704–11